

Auroral Radio Source Occultation Modeling and Application to the JUICE Science Mission Planning

B. Cecconi¹, C. K. Louis², C. Muñoz Crego³, and C. Vallat⁴

¹ LESIA, Observatoire de Paris, CNRS, PSL Research University, Meudon, France
e-mail: baptiste.Cecconi@observatoiredeparis.psl.eu

² School of Cosmic Physics, DIAS Dunsink Observatory, Dublin Institute for Advanced Studies, Dublin 15, Ireland
e-mail: corentin.louis@dias.ie

³ Aurora B.V., for European Space Agency, ESAC, Madrid, Spain
e-mail: cmunoz@sciops.esa.int

⁴ Rhea Group, for European Space Agency, ESAC, Madrid, Spain
e-mail: cvallat@sciops.esa.int

ABSTRACT

Aims. Validate the use of ExPRES as an observation planning tool for the JUICE mission.

Methods. We simulate the occultations of the Jovian auroral radio emissions during the Galileo flybys of the Galilean moons of Jupiter. The ExPRES simulations runs are configured using fixed typical parameters for the main aurora radio emissions. We compare the simulation run results with the actual Galileo PWS observations.

Results. The ExPRES code accurately models the temporal occurrence of the occultations in the whole spectral range observed by Galileo PWS.

Conclusions. The method can be applied for preparing the JUICE moon flyby science operation planning.

Key words. radio continuum: planetary systems emissions – planets and satellites: individuals: Jupiter – planets and satellites: individuals: Io – planets and satellites: individuals: Europa – planets and satellites: individuals: Ganymede – planets and satellites: individuals: Callisto

1. Introduction

The magnetosphere of Jupiter produces low frequency radio emissions from its polar regions, along the active magnetic field lines connected to the Jovian auroral oval as well as to the Galilean moon auroral magnetic footprints. The Jovian radio emissions are intense and non-thermal radio frequency phenomena, spanning from a few kHz to about 40 MHz, and produced through the Cyclotron Maser Instability (CMI), which converts the local plasma free-energy into electromagnetic radiation (Zarka 1992). They are used as a proxy for the Jovian magnetospheric activity. They have been discovered by Burke & Franklin (1955) and have been since studied with ground observatories (e.g., Nançay Decameter Array, Lamy et al. 2017) and space-borne instruments (with, e.g., the Voyager, Galileo, Cassini and Juno space missions).

Observations from the Cassini Radio and Plasma Waves Science (RPWS, Gurnett et al. 1992) and Galileo Plasma Waves Science (PWS, Gurnett et al. 1992) experiments showed that the Jovian radio emission events are observed quasi-permanently along the spacecraft orbit. Figure 1 shows 24 hours of simultaneously observed spectral flux densities by the Cassini/RPWS and Galileo/PWS instruments, when Cassini was close to its flyby of Jupiter. Both panels of this figure display many arc-shaped radio events (a few of them are highlighted with a thin plain black line), with a few small time-frequency regions with quiet (background level) conditions. Radio arcs can be classified with orientation of their curvature: “vertex-early” and “vertex-late” arcs corresponds to opening “(” or closing “)” parenthesis shapes.

The arc shape of Jovian radio emission is well explained by the CMI mechanism at the radio source, coupled with the shape of the magnetic field lines, and the rotation of Jupiter with respect of the observer, as described in Fig. 1 of Louis et al. (2019). This figure also introduce two other features of the observed radio spectrum around Jupiter: Type II Solar radio bursts are also observed depending on the solar activity (three events are highlighted with a thin dashed black line); and the so-called “attenuation lanes” (Gurnett et al. 1998) resulting from the propagation of hectometric waves through the Io plasma torus (Menietti et al. 2003). The attenuation lanes are observed as a narrow-band attenuation feature modulated at the planetary rotation period. The attenuation is also accompanied or replaced with an intensification of the signal, similarly to caustic optical phenomena.

Although not covering the full spectral range of the Jovian radio emissions, Galileo/PWS has been routinely collecting radio observations during its many orbits in the Jovian system. This data (Gurnett et al. 1997) shows quasi continuous emission from a few 100 kHz up to 5.6 MHz, the upper spectral limit of PWS. During the Galilean moon flybys, Galileo/PWS observed full occultations of the Jovian radio emissions (Kurth et al. 1997).

The ESA JUICE (JUperiter ICy moon Explorer, Witasse 2019) will explore the Jupiter system and its magnetosphere. The study of the Jovian magnetosphere can strongly benefit from remote observations and modelling tools (Cecconi 2019). Two instruments of the JUICE scientific payload are operating in the low frequency radio range (below 50 MHz): the Radio and Plasma Waves Instrument (RPWI, Wahlund 2013) has a receiver ded-

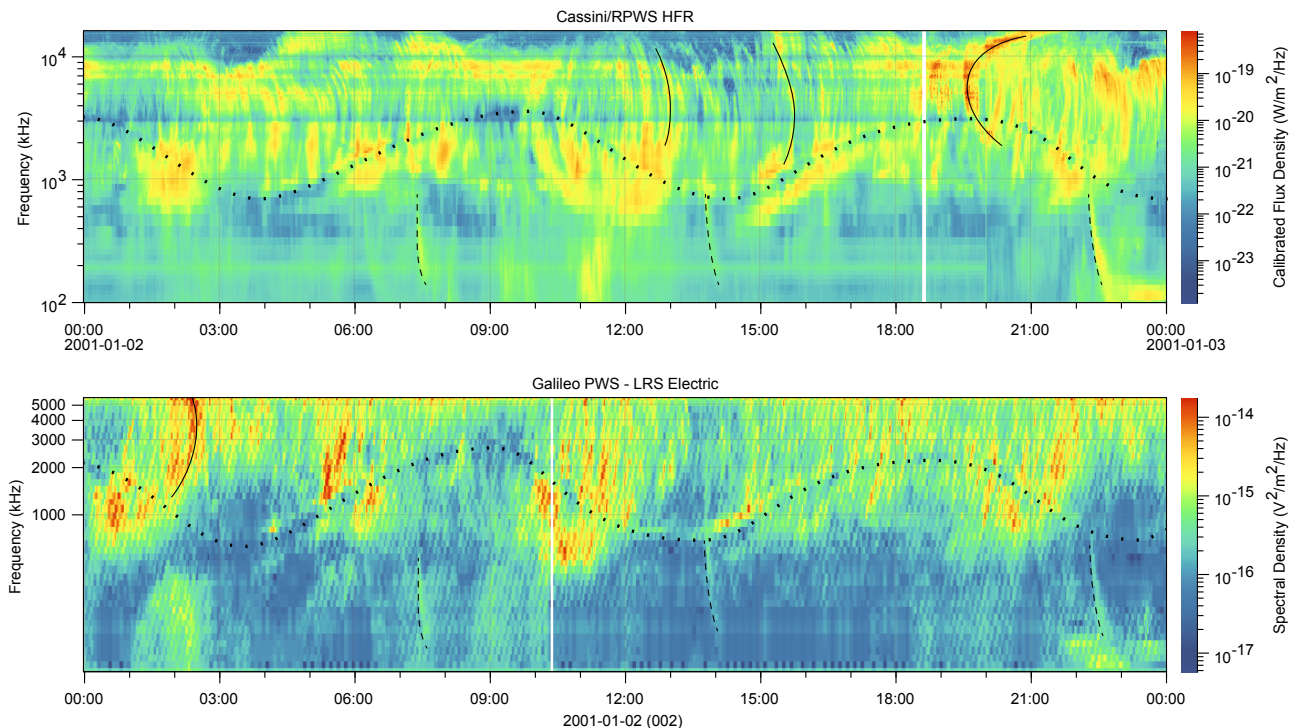


Fig. 1. Calibrated Cassini/RPWS/HFR (Zarka et al. 2004; Cecconi & Zarka 2019) (top) and GLL/PWS (see Section 2.1) (bottom) radio electric power spectral densities during 24 hours close to the Cassini flyby of Jupiter. Significant features have been highlighted: a few radio emission “arcs” are traced in plain line; Type III Solar radio bursts are traced in dashed line; and the attenuation lanes are traced in dotted line.

icated to the study of Jovian radio emissions; and the Radar for Icy Moon Exploration (RIME) experiment (Bruzzone et al. 2013) is operating with a central frequency at 9 MHz, which lies within the Jovian radio emission spectral range. The Jovian radio emission may interfere with RIME active radar mode (Cecconi et al. 2012), but can be also used in a passive radar experiment mode during icy moon flybys (Romero-Wolf et al. 2015; Schroeder et al. 2016; Kumamoto et al. 2017).

The ExPRES code (Exoplanetary and Planetary Radio Emissions Simulator, Louis et al. 2019) simulates for a given observer the geometrical visibility of radio emissions of a magnetised body. This visibility depends in particular of the emission angle between the magnetic field vector at the source and the emitted wave vector, which is computed self-consistently in the frame of the CMI theory. The anisotropic shape of the radio source and their geometrical observability conditions are well described in Fig. 1 (panels c, d and e) of Louis et al. (2019). This computation is iterated at each time/frequency step and for each source. The produced time-frequency map (or dynamic spectrum) can then directly be compared to observations.

In this study, we are modelling the Jovian radio emission occultations during (past) Galileo and (planned) JUICE Galilean moon flybys, using the ExPRES code.

2. Data Sets

Several sets of data have been used in this study and are presented in this section. For the Galileo spacecraft flybys, we compare the actual observed radio spectra, with low frequency radio occultations predicted by the ExPRES code, using the actual

flyby geometry (spacecraft and moon trajectory in a Jovian reference frame). The JUICE spacecraft study only includes modelled occultation.

2.1. Galileo PWS Observations

All Galilean moon flyby of Galileo with PWS data have been modelled and analysed. The Galileo PWS (hereafter referred to as GLL/PWS) data have been retrieved from University of Iowa *das2* server interface (Piker et al. 2019), using the *das2py*¹ python module. We have used the *GLL/PWS LRS 152-channel calibrated electric* collection² from that *das2* server. The data are radio-electric power spectral densities provided in units of $V^2/m^2/Hz$. This dataset doesn’t include the instrument’s antenna gain calibration, but this has no consequence on this study. The data set has a native time resolution of 18.67 seconds. These data are also available in the full resolution GLL/PWS dataset (GO-J-PWS-2-REDR-LPW-SA-FULL-V1.0, Gurnett et al. 1997), at NASA PDS (Planetary Data System) PPI (Planetary Plasma Interaction) node.

2.2. Moons and Spacecraft Trajectory Data

The moons and spacecraft trajectory data are computed using SPICE kernels (Acton 1996). In this study, the ephemeris data have been retrieved using the NASA-JPL (Jet Propulsion Labo-

¹ currently available from <https://github.com/das-developers/das2py>

² http://das2.org/browse?resolve=tag:das2.org,2012:site:uiowa/galileo/pws/survey_electric

ratory of the National Aeronautics and Space Administration) instance of WebGeocalc (Acton et al. 2018) for Galileo spacecraft and Jovian moons, and another WebGeocalc instance at ESA-ESAC (European Space Astronomy Centre of the European Space Agency) for the JUICE spacecraft. The JUICE spacecraft SPICE kernels (ESA SPICE Service 2020) contains all the studied orbital scenarios, as described in the JUICE CReMA (Consolidated Report on Mission Analysis) documents. In this study, the selected JUICE trajectory scenario is CReMA-3.0. The ephemeris of all bodies have been retrieved in the IAU_JUPITER reference frame, also referred to as “IAU Jupiter System III (1965)”. In the WebGeoCalc interface, we use the “planetocentric” representation for coordinate retrieval, in which the longitude is oriented Eastward.

For each flyby, two ephemeris data files are retrieved, using the ‘State Vector’ WebGeocalc capability: (a) the location of the moon and (b) that of the spacecraft, both in the IAU_JUPITER frame, as seen from the center of Jupiter, with a time interval of a few hours (2 to 4 hours, depending on the spacecraft velocity relative to the moon) centred on the closest approach epoch of the flyby, and a time sampling step of one minute. We do not correct for light time propagation. The resulting uncertainty in ephemeris data timing is of the order of 1 second, which is much below time resolution of the data and the simulations.

3. Jovian Radio Emissions Occultations

As shown by Kurth et al. (1997), the Jovian hectometric radio emissions are occulted by Ganymede during G01 flyby (Ganymede flyby during the first orbit around Jupiter) of the Galileo spacecraft, on June 27th 1996. Figure 1 of Kurth et al. (1997) shows the GLL/PWS spectrogram during G01 flyby (also displayed on the bottom-left panel of Figure 2). The full occultation is observed between 05:50 and 06:20 SCET. The occultation spectral ingress and egress profiles imply that the observed radio sources at higher frequencies (located close to Jupiter) are occulted earlier and reappears later than the lower frequency ones, which are located further out from Jupiter. Possible occultation of the Jovian radio emissions have been also reported during the first Io flyby of Galileo (Louarn et al. 1997).

Table 1 shows our assessment of all targeted Galilean moon flybys by the Galileo spacecraft. Appendix B provides access to the full material used to conduct this study, with figures corresponding to each flyby. In this paper, we have selected one flyby of each Galilean moon, where the radio emission occultation was clearly observed (see the grey rows in Table 1). Figure 2 shows GLL/PWS observations for each of the selected flybys, i.e., from left to right and top to bottom: Io (I24), Europa (E12), Ganymede (G01) and Callisto (C30) flybys.

3.1. Radio Emission Modeling

We model the location of the Jovian auroral radio sources visible at Galileo’s location using ExPRES (version 1.1.0, Louis et al. 2020)). Our simulation runs are configured as follows: (a) we use the JRM09 magnetic field model (Connerney et al. 2018) together with the Connerney et al. (1981) current sheet model; (b) the sources are set every 1° in longitude along active magnetic field lines of $M_{\text{shell}} = 30$ (M_{shell} being the measure of the magnetic apex, i.e., the distance in Jovian radii (R_J), of the magnetic field line at the magnetic equator), corresponding to the main auroral oval (Grodent 2015); (c) the unstable electron temperature is set to 5 keV (Louarn et al. 2017); and (d) the location of the visible radio sources is modeled with a temporal step of one

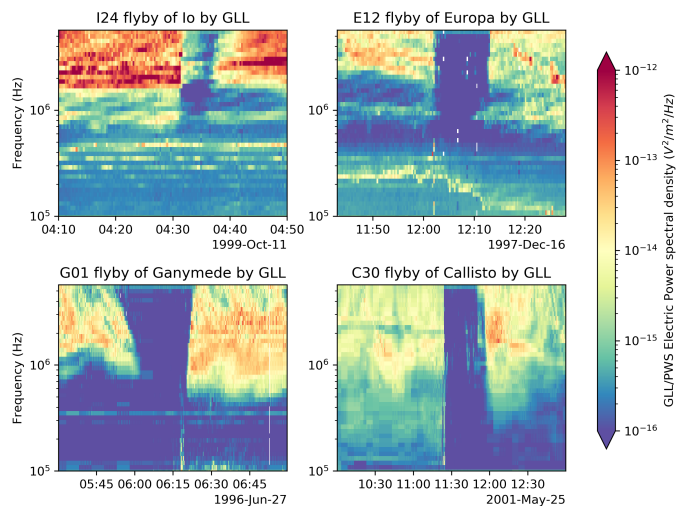


Fig. 2. Jovian radio emission occultations by Io (upper left), Europa (upper right), Ganymede (lower left) and Callisto (lower right), as seen by GLL/PWS. The figures are showing radio electric power spectral densities in $\text{V}^2/\text{m}^2/\text{Hz}$.

minute. These parameters are fixed for all simulation runs used in this study. We also included Io-induced radio emissions in the simulation runs, with the same unstable electron distribution temperature (5 keV). The ExPRES configuration file is available, as described in appendix B.

When the observer is located near the magnetic equator, the radio source beaming pattern implies that the visible radio source are split into four cluster locations, called A, B, C and D, corresponding respectively to the North-Eastern, North-Western, South-Eastern and South-Western quadrant around Jupiter as seen from the observer (see, e.g., Fig. 2 of Marques et al. 2017, for a definition).

The simulation runs have been computed using the OPUS Servillat et al. (Observatoire de Paris UWS Server, 2021a)) instance operated by PADC³ for the MASER (Measurement, Analysis and Simulation of Emissions in the Radio range) project (Cecconi et al. 2020). OPUS is a framework running the Universal Worker Service (UWS) protocol (Harrison & Rixon 2016). The ExPRES code is available for run-on-demand from this interface⁴.

3.2. Occultation Modeling

The occultation is computed using a simple geometric derivation of the intercept distance between the center of the Galilean moon and the straight lines passing by each visible modelled radio source and the observer. Any source with an intercept distance shorter than one moon radius is occulted, assuming a spherical moon, as sketched on Figure 3.

4. Observations

All Galileo flybys have been analysed and modelled using ExPRES. In this section, we present the detailed modelling results corresponding to the highlighted rows of Table 1. Figures 4, 5, 6 and 8 present the results for these four flybys. The flybys are presented in order to show the simpler to the more complex cases.

³ Paris Astronomical Data Centre: <https://padc.obspm.fr>

⁴ UWS MASER portal: <https://voparis-uws-maser.obspm.fr/client/>

Orbit Name	Moon Name	Moon Closest Approach	Data Availability		Occultation Assessment
			GLL/PWS	SPICE	
I00	Io	1995-12-07 17:45:58	yes	yes	(?)
G01	Ganymede	1996-06-27 06:29:07	yes	yes	yes
G02	Ganymede	1996-09-06 18:59:34	yes	yes	(?)
C03	Callisto	1996-11-04 13:34:28	yes	yes	(?)
E04	Europa	1996-12-19 06:52:58	yes	yes	no
E06	Europa	1997-02-20 17:06:10	yes	yes	(?)
G07	Ganymede	1997-04-05 07:09:58	yes	yes	(?)
G08	Ganymede	1997-05-07 15:56:10	yes	yes	yes
C09	Callisto	1997-06-25 13:47:50	yes	yes	(?)
C10	Callisto	1997-09-17 00:18:55	yes	yes	no
E11	Europa	1997-11-06 20:31:44	yes	yes	no
E12	Europa	1997-12-16 12:03:20	yes	yes	yes
E14	Europa	1998-03-29 13:21:05	yes	yes	(?)
E15	Europa	1998-05-31 21:12:57	yes	no	yes
E16	Europa	1998-07-21 05:03:45	yes	yes	(?)
E17	Europa	1998-09-26 03:54:20	yes	yes	(?)
E18	Europa	1998-11-22 11:38:26	no	yes	—
E19	Europa	1999-02-01 02:19:50	yes	yes	(?)
C20	Callisto	1999-05-05 13:56:18	yes	yes	no
C21	Callisto	1999-06-30 07:46:50	yes	yes	no
C22	Callisto	1999-08-14 08:30:52	yes	yes	yes
C23	Callisto	1999-09-16 17:27:02	yes	yes	yes
I24	Io	1999-10-11 04:33:03	yes	yes	yes
I25	Io	1999-11-26 03:59:15	yes	yes	(?)
E26	Europa	2000-01-03 17:59:56	yes	yes	no
I27	Io	2000-02-22 13:46:36	yes	yes	yes
G28	Ganymede	2000-05-20 10:10:18	yes	yes	no
G29	Ganymede	2000-12-28 08:25:27	yes	yes	no
C30	Callisto	2001-05-25 11:23:58	yes	yes	yes
I31	Io	2001-08-06 04:59:21	yes	yes	no
I32	Io	2001-10-16 01:23:21	yes	yes	(?)
I33	Io	2002-01-17 14:08:23	yes	yes	(?)

Table 1. List of all targeted Galilean moon flybys with PWS/Electric-Survey data. The data from all flybys (except E18) are available through the University of Iowa *das2* server end-point. The spacecraft ephemeris data is available for all flybys except E15. The occultation assessment indicates if the occultation is observed (*yes* or *no*) or unsure (?). The grey lines correspond to the flybys shown in Figure 2 and described in details in this study. Table adapted from Table 1 (Orbital Facts) of the CATALOG/GO_MISSION.CAT label file available from Gurnett et al. (1997)

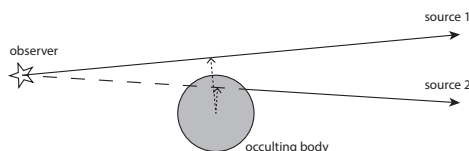


Fig. 3. Simple geometric occultation scheme used in this study. The interception distance (dotted segment) is computed as the distance between the center of the occulting body and the line of sight between the observer and the source. In this case the source 1 is not occulted, while source 2 is.

The GLL/PWS data (same data as in Figure 2) are plotted together with the simulations of observable auroral radio emissions (described in Section 3.1) separated into the four source types A, B, C and D (from white to black, respectively). The comparison of observations and modelled data shows that the simulations reproduce the Jovian radio occultation during the four flybys presented in Figure 2.

Appendix B describes the supplementary material available for all flybys (Cecconi et al. 2021), which contains all the material used to conduct this study. For each Galileo flyby, we provide: (a) a figure showing the GLL/PWS data and the observable

radio sources modeled by EXPRES, and (b) movies showing a subset of Jovian radio sources (a selected sub-set of frequencies), as seen from Galileo ('pov' movies), or from the top of the Jovian system ('top' movies).

4.1. Callisto C30 flyby

The occultation occurring during the C30 flyby of Callisto is displayed in Figure 4. The ingress occultation time is very well reproduced (within one minute accuracy). All sources are occulted simultaneously, with radio emissions intensity dropping instantly, at $\sim 11:25$ SCET. At egress, we observe first a faint rise of the emission intensity from $\sim 11:50$ to $\sim 12:00$, and then a sudden return to maximum intensity at $\sim 12:00$. This egress phase can be visualised in the supplementary material available for this flyby: <https://doi.org/10.25935/8ZFF-NX36#C30>. The frames between 11:44 to 11:59 of the 'pov' movie clearly shows the various sources reappearing one after the other: first, the B sources, then the A and D sources simultaneously and finally the C sources. The predicted reappearance of C sources perfectly coincides with the observed full egress phase. This leads to two observations: (i) the main radio contribution is that of the C sources at the time of observation,

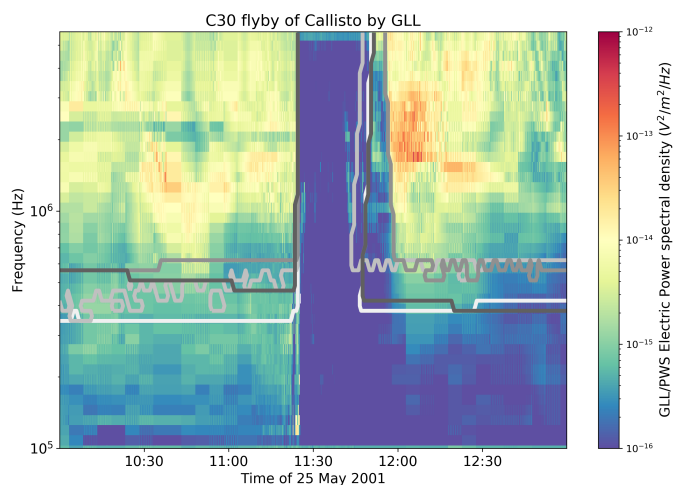


Fig. 4. Superimposed GLL/PWS data and ExPRES simulations during Jovian radio emission occultations by Callisto (flyby C30). The four types of emission (A, B, C, D) are separated (from white to dark grey, resp.)

and (ii) the radio sources are occulted by the moon’s surface (or very close to it).

The low-frequency cut-off is not perfectly simulated (especially on the ingress side), with a difference of about 200 kHz. This lower frequency limit is mostly due to the ratio of the plasma and cyclotron electronic frequencies in the radio source, as configured in the ExPRES simulations. The error of a few 10s-100s kHz is thus probably due to an incorrect estimation of the electron density around Jupiter. An attenuation feature is observed starting at ~ 2.5 MHz, and decreasing to ~ 2 MHz at ingress. This corresponds to the attenuation lanes described in the introduction section. In addition, during the full occultation period of time, faint and sporadic signals are observed between ~ 800 kHz and ~ 2 MHz.

4.2. Europa E12 flyby

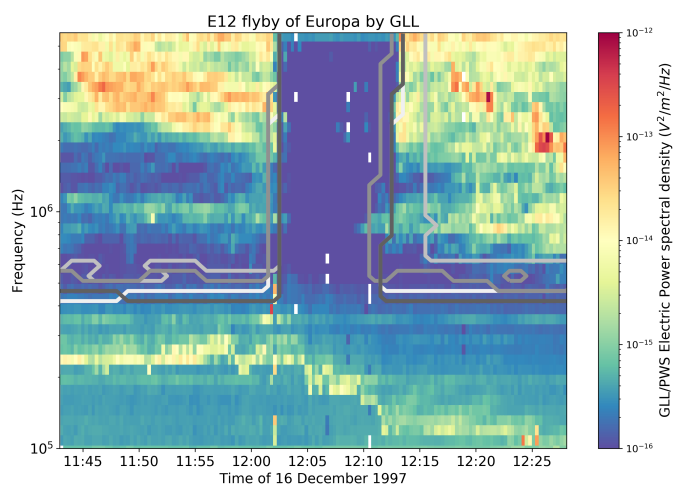


Fig. 5. Superimposed GLL/PWS data and ExPRES simulations during Jovian radio emission occultations by Europa (flyby E12). The four types of emission (A, B, C, D) are separated (from white to dark grey, resp.)

The E12 Europa’s flyby (Fig. 5) is similar to C30 Callisto’s flyby case, where all sources are occulted simultaneously at ingress. Faint and sporadic radio signatures are observed during the full occultation phase (as in the case of C30). At egress, the simulation well reproduces the end of the occultation, except in the $\approx [800-1000]$ kHz frequency range where we observed emission during the modelled occultation.

The attenuation lane feature is observed at and below ~ 2 MHz before ingress, with a corresponding feature after egress, up to $\sim 12:20$. At about ~ 1 MHz, an intensification is also observed, before ingress and after egress (corresponding to the aforementioned prediction mismatch), and is probably linked to the attenuation lanes.

The spectral line observed between ~ 250 kHz (at the beginning of the interval) and ~ 100 kHz (at the end) corresponds to the local plasma upper-hybrid frequency line ($f_{UH} = \sqrt{f_{pe}^2 + f_{ce}^2}$, where f_{pe} and f_{ce} are the local plasma, and electron cyclotron frequencies, respectively).

4.3. Ganymede G01 flyby

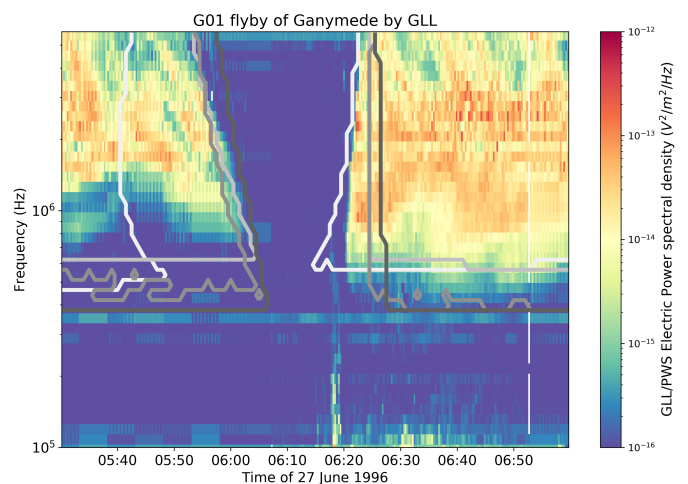


Fig. 6. Superimposed Galileo PWS data and ExPRES simulations during Jovian radio emission occultations by Ganymede (flyby G01). The four types of emission (A, B, C, D) are separated (from white to dark grey, resp.)

Figure 6 displays the occultation modeling of the Jovian radio emissions during the G01 flyby of Ganymede. At ingress, unlike the previous two cases, all sources are not occulted simultaneously. First the A sources are occulted, then the B, C and D sources, with the beginning of the full occultation. Before observed egress, a broadband noise burst at $\sim 06:18$, going up to ~ 800 kHz. This has been interpreted as the signature of Ganymede’s magnetopause crossing by Gurnett et al. (1996). At egress, the modelled reappearance of the A sources (white line) well reproduce the end of the observed occultation at frequencies higher than a few MHz. At lower frequencies, the egress occurs later than predicted. At ~ 700 kHz, it is observed at $\sim 06:21$, and predicted at $\sim 06:16$.

During this flyby, the radio sources are not occulted simultaneously at both egress and ingress, and not at the same time on the whole spectral range, which is due to the trajectory of Galileo. Figure 7 shows a modelled image, from the Galileo spacecraft point of view, at the beginning of the G01 occultation sequence. This frame is extracted from the G01 movie available

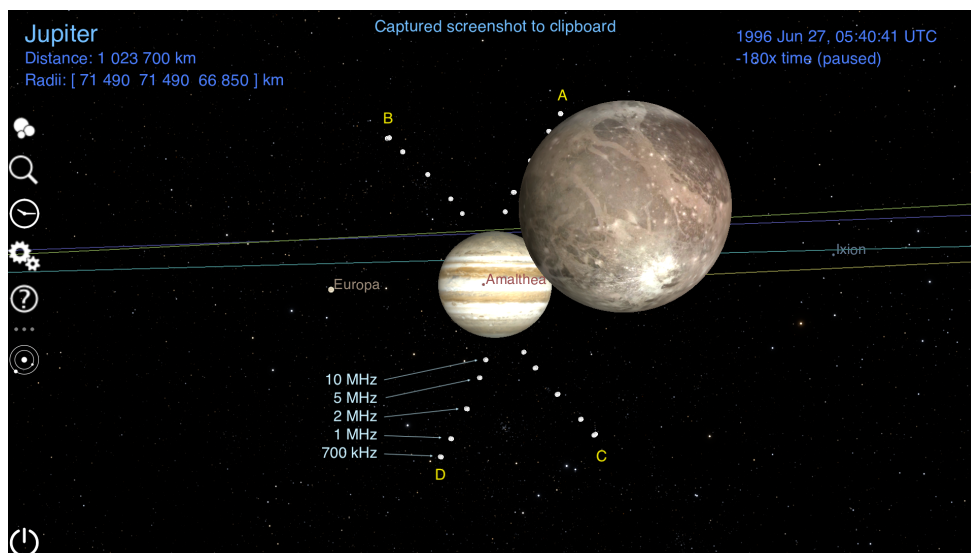


Fig. 7. G01 Flyby visualised in the Cosmographia tool. The scene is set with an observer on the Galileo spacecraft, pointing to Jupiter. Ganymede is in the field of view. The ExPRES-modelled visible radio sources are also shown, at 700 kHz, 1 MHz, 2 MHz, 5 MHz and 10 MHz. The radio sources are naturally grouped in four sets (named A, B, C and D). A the time of the snapshot (1996-06-27T05:40:41 UTC), Ganymede is occulting the radio source at 2 MHz in the A-group.

in supplementary material at: <https://doi.org/10.25935/8zfff-nx36#G01>.

4.4. Io I24 flyby

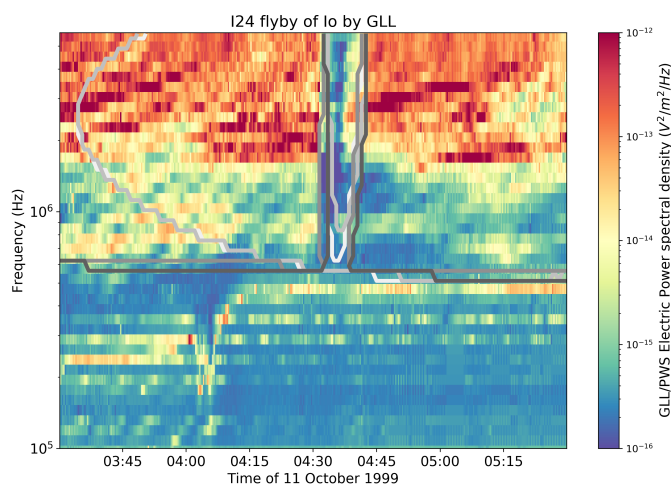


Fig. 8. Superimposed GLL/PWS data and ExPRES simulations during Jovian radio emission occultations by Io (flyby I24). The four types of emission (A, B, C, D) are separated (from white to dark grey, resp.)

Figure 8 displays the occultation during the I24 Io’s flyby. At ingress, the occultation of the higher intensity is well modelled. We observe radio signals during the modelled full occultation, and the observed egress seems to occur earlier than the prediction. Intense radio arcs are visible above 2 MHz, showing the lower frequency part of vertex-late arcs. The radio signal is attenuated below 1 to 2 MHz, especially after the flyby. The f_{UH} line is also observed (~ 300 kHz to ~ 500 kHz).

This Io flyby also shows a noticeable feature. The modelled Northern radio sources (A and B, respectively in white and light-grey) are not observed at the beginning of the studied interval. This is due to the “Equatorial Shadow Zone” (ESZ) effect re-

ported at Saturn (Lamy et al. 2008), see Appendix A for more details.

4.5. Other flybys

In the case of flybys with partial occultations (e.g., G02, G07, E11, E26 or G28), the Jovian radio signals are observed during the flyby, with no full occultation interval. During the G07 flyby, only D sources are occulted. The GLL/PWS data (see <https://doi.org/10.25935/8zfff-nx36#G07>) shows an attenuation of the Jovian radio signals that fits the predicted occultation (see Figure 9), hence suggesting that several radio sources were active, including the D sources.

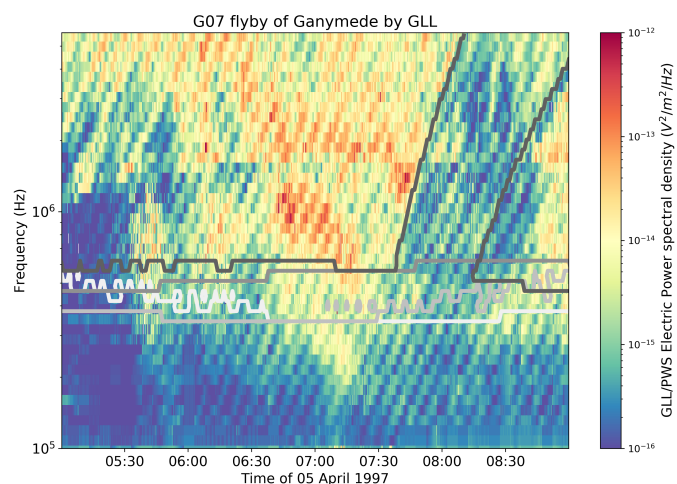


Fig. 9. Superimposed Galileo PWS data and ExPRES simulations during Jovian radio emission occultations by Ganymede (flyby G07). The four types of emission (A, B, C, D) are separated (from white to dark grey, resp.)

Most of the other flybys (e.g., C03, E04, E06, G08, C10, E19) are occurring on the Jovian-facing side of the moon, where no occultation can occur.

5. Results and Discussion

The first result of this study is the fact that Jovian auroral radio emissions are present almost continuously, although this may not be obvious in some observational data sets, due to the limited sensitivity of instruments. Ground based radio telescopes (such as the Nançay Decameter Array, in France) provide the longest observation collections (Marques et al. 2017), but the distance to Jupiter limits the detection of low intensity events despite their intrinsic sensitivity. Space borne radio instruments (such as Voyager/PRA, Cassini/RPWS, GLL/PWS or Juno/Waves), provide observations from a closer range to Jupiter. Cassini and Galileo data show quasi-continuous radio signals (as shown on Figure 1). The ExPRES modeling of auroral radio sources, configured with radio sources every 1° in longitude, is consistent with this observation (with the noticeable exception of the ESZ, for an observer located around Io's orbital distance to Jupiter). The occultation modeling analysis shows that all sources must be occulted in order to remove the natural radio signature of Jupiter's magnetospheric activity. It is also noticeable that faint emissions are still visible during some occultations (e.g., during the G01, E12 and C30 Galileo flybys).

The JUICE/RPWI and RIME instruments will observe similar radio signal levels. The JUICE/RIME and Cassini/RPWS instruments have similar antenna characteristics, leading to an antenna resonance at about ~ 9 MHz (Zarka et al. 2004; Bruzzone et al. 2013). It is thus very likely that JUICE/RIME will observe similar signals as those shown on Figure 1 (with a spectral range restricted around 9 MHz).

The low frequency limit is usually well predicted by ExPRES, as shown on Figures 4, 5, 6, 8 and 9. The ExPRES low frequency emission limit is determined by the CMI theory: the emission can occur only when $f_{pe}/f_{ce} < 0.01$. This finding implies that our modeling of the magnetic field and plasma density is consistent with the radio observations. Discrepancies (e.g., during flyby C30) may be related to the modeling of the two aforementioned characteristic frequencies: f_{pe} depends on the magnetospheric current sheet model; and f_{ce} is determined by the magnetic field model. The JRM09 magnetic field model is derived from the Juno magnetic measurements in the polar regions of Jupiter. This model is thus perfectly adapted for our application. Conversely, the current sheet model could be improved. The results of this study will be checked and updated if needed when a new model is published. The effect of the Solar Wind conditions may also play a role (as studied by Hess et al. 2012), but the influence at the lowest frequencies remains to be studied.

Figure 10 displays the occultation of the Jovian radio sources during the flyby I24, for two sets of simulation runs. In the top and bottom panels, the sources are located on the magnetic field lines with an M-shell of 50 and 30 R_J , respectively, with the larger M-shell, corresponding to radio sources located at higher magnetic latitudes. We observe no difference for the occultation prediction. The difference in the low cut-off frequency of the simulated emissions is very small (with a slightly lower low cut-off frequency for sources with M shells of 50 R_J). The main difference is observed for the A and B sources (white and light-grey curve), with the ESZ feature occurring at a different time.

The ExPRES modeling results show that the occultation modeling is predicting accurately the observed occultation (e.g., C30 flyby, or E12 and I24 flyby ingress). The ExPRES simulation runs have been configured with a 1 minute sampling step, which sets the general temporal accuracy of this study. The discrepancies between the predictions and observation have

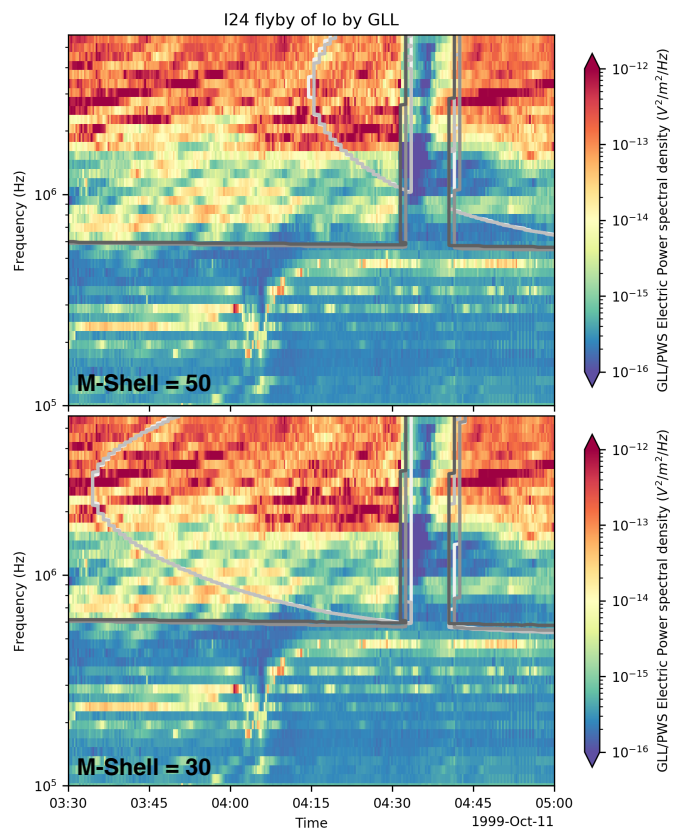


Fig. 10. Comparison between the jovian radio occultation during the I24 flyby for sources on magnetic field lines at M shell $M=50$ (top panel) and $M=30$ (bottom panel).

to be further studied. The mismatch mostly occurs at frequencies lower than ~ 1 MHz. In this range, propagation effects (such as refraction effects) are known to occur, with, e.g., attenuation lanes. We observe them in all studied flybys, e.g., on E12, where the Jovian auroral radio waves are attenuated below ~ 2 MHz, with an intensification at ~ 1 MHz.

In the case of G01, the egress is observed several minutes after the predicted egress time. If we don't consider refraction, the radio waves are propagating along a straight line, and the altitude of the radio source above the limb when they reappear would provide the upper limit of f_{pe} along this line. From G01, the radio source at 600 kHz reappears at 06:21 SCET, which corresponds to an altitude of ~ 300 km above the Ganymede's limb. The observation frequency would translate into a plasma density of about 4500 cm^{-3} . The same analysis for the radio source at 2 MHz leads to an estimation of $\sim 10^5 \text{ cm}^{-3}$ close to the moon's surface. This value is inconsistent with previously published plasma density models for Ganymede environment (Gurnett et al. 1996; Kliore 1998; Eviatar et al. 2001). Figure 11 shows how the same observations can be interpreted considering refraction effects on the ionosphere of the moon.

In Figures 4, 5 and 6, we observe faint and sometimes sporadic radio signals, which are visible during the occultation interval, despite the predicted full occultation. Since the moon is geometrically occulting all the Jovian radio sources, refraction effects must be taken into account to interpret the observation. These effects can occur either in the moon's atmosphere and ionosphere, in the Io plasma torus or in the magnetospheric plasma sheet. ExPRES assumes a straight line propagation between the radio source and the observer.

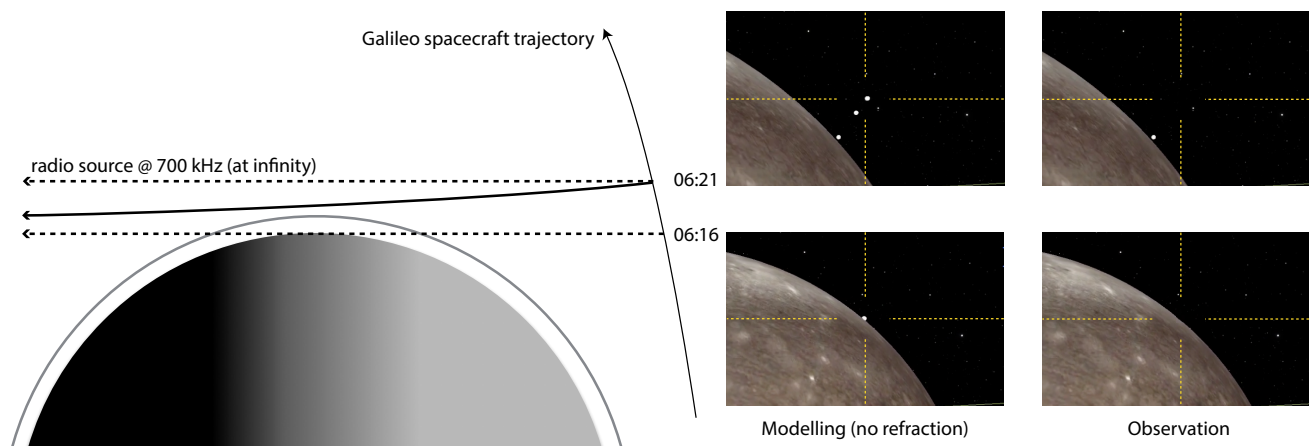


Fig. 11. Sketch of G01 configuration, with a modelled radio source at 700 kHz, assumed to be at infinity on the left-hand side. The plain line is a sketched refracted ray path. The plain grey line represents the ionosphere of the moon. The dashed lines are the straight line propagation (no refraction) for the same source. Two locations of the Galileo spacecraft trajectory are illustrated on the right-hand side of the Figure. The “Modelling (no refraction)” column shows frames extracted from the G01 ‘pov’ movie at 06:16 and 06:21. The right-most column (“Observation”) shows the radio source visibility, including refraction effects at low frequencies.

The two latter results (occultation ingress and egress prediction mismatch and faint signals during full occultation) indicate that propagation effects play an important role in the fine understanding of the Galilean radio occultations. Further analysis requires the coupling to a ray-tracing code, such as ARTEMIS-P (*Anisotropic Ray Tracer for Electromagnetism in Magnetosphere, Ionosphere and Solar wind including Polarization*, Gautier et al. 2013).

6. Usage for the JUICE mission planning tools

The science planning activity, coordinated by the JUICE Science Operations Center, relies on the identification at each point in time of the science observations opportunities, using science models or/and geometry. For JUICE, some of those opportunity periods depend on the Jupiter Radio emission simulation; ionosphere characterization, active and/or passive radar sounding activities opportunities can benefit from an accurate simulation of Jupiter radio emission.

Since the ExPRES Tool can provide as by-product the positions of the radio sources as seen from the spacecraft for a range of frequencies (i.e., 1-40 MHz), the Juice Science Operation Centre (JUICE SOC) has implemented a standalone tool, which wraps the ExPRES tool and identify science opportunity windows based on the radio source position.

This can be used to identify opportunity windows for one of the high priority science objectives of the Juice RPWI instrument, the icy moon ionosphere characterization through ionosphere refraction/distortion measurement.

The opportunity periods currently generated to drive the corresponding RPWI measurements are linked to the ingress and egress occultation events of the Jupiter Radio Sources, where at least one Jupiter radio sources reach Juice spacecraft with a frequency between 0.1-5 MHz crossing the moon ionosphere (with thickness 0-100km).

In the figure 12, the Jupiter auroral radio source as seen from JUICE during 21C13 (the last Callisto flyby of the tour) as a function of frequency (MHz) and UTC time is displayed: the red dots correspond to opportunity for ionosphere characterization, i.e., whenever one of the radio source types (A, B, C or D) is seen by JUICE with a line of sight passing through the ionosphere

within 0-100 km. This section is using the CReMA 3.0 trajectory scenario.

Figure 13 shows the resulting ionosphere characterization opportunities as a function of the Juice spacecraft altitude in km (green background). There are a few gaps within the ingress and egress ionosphere characterization opportunities. Those gaps of 1-2 minutes are ignored to compute the final `iono_ingress` and `iono_egress` envelopes used for the observations planning. Table 2 lists the RPWI in-situ and radio measurement sequence for the 21C13 scenario based on the Closest Approach (CA), and the ingress and egress windows envelope for ionosphere characterization.

Finally figure 14 is a screenshot of this measurement sequences as shown by the JUICE SOC Mapping and Planning Payload Science software (MAPPS), used to simulate the spacecraft and payload resources status (i.e., power, data rate, on-board solid-stat mass memory (SSMM)). The RPWI operations are planned around the CA and around ingress and egress ionosphere characterization opportunities as described in Table 2. The high-resolution in-situ measurement mode is scheduled +/- 10 minutes around the closest approach (CA), while the high resolution radio measurement mode is scheduled during the ionosphere characterization opportunities. High-resolution modes are the more demanding in term of resources (power, data generated, stored in SSMM and to be downloaded (data rate)) and there are reserved for priority scientific objectives. So it is crucial to be able to calculate the corresponding opportunities windows.

The JUICE mission is in development phase, with a planned launch in June 2022. At this stage the JUICE mission science planning process is being exercised by analyzing representative science scenarios similar to 21C13. In this study, the scenario analysis covers ± 12 hours around the Callisto closest approach.

The JUICE SOC is identifying the same type of opportunity windows whenever a new candidate trajectory is available for JUICE.

The ExPRES tool simulation results can also be useful for other measurement types, and will be made available for by JUICE SOC instrument teams. This includes the measurement linked to the icy shell characterization of the icy moons:

- Passive radar measurement by the radar (RIME instrument) or by RPWI: Opportunities can be identified whenever any

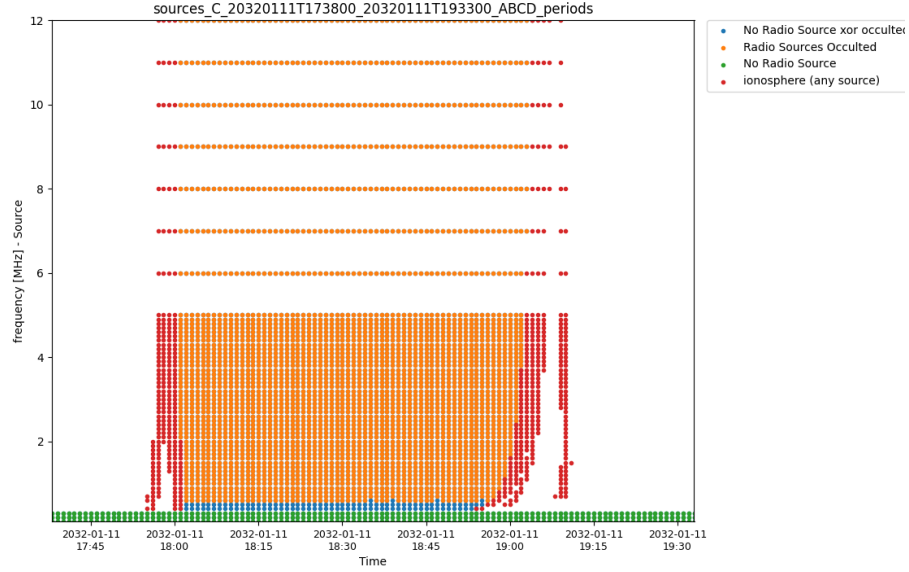


Fig. 12. dots represent the Jupiter auroral radio source state as a function of frequency (MHz) and UTC time for the last Callisto flyby (21C13). Red dots means that at least one of the source type (A, B, C and D) is visible from JUICE and that the line of sight between the source and the spacecraft goes through the ionosphere within 0-100 km altitude above Callisto surface. The blue, orange and green dots mean that no radio source is visible by JUICE at those frequency ranges. Here "No Radio Source" means that there is no emission from the corresponding source; Jupiter ionosphere does not generate emissions at high frequencies while emissions at low frequencies are too weak, and therefore do not produce emissions.

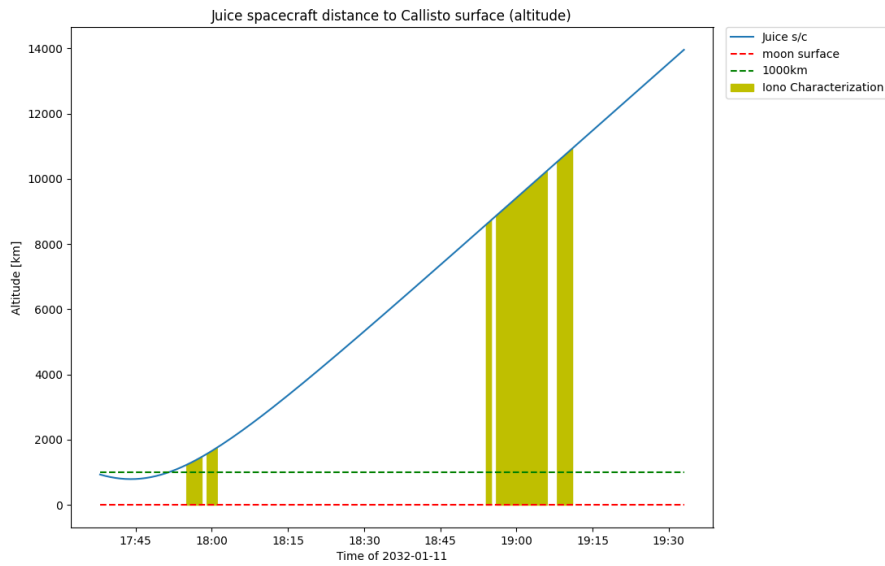


Fig. 13. Juice spacecraft distance to the Callisto moon surface in km for the 21C13 Flyby (blue line); the Callisto surface (resp. the 1000km altitude above surface) is represented by the red dashed line (resp. green dashed line), and the ionosphere characterization opportunities windows are filled in greenish background.

radio source is visible from the spacecraft for any source type (ABCD), and per source type (to differentiate source from north and south hemisphere) between 1 and 40 MHz (although lower frequencies are better since they have a deeper penetration into the ice);

- Active Radar measurement by the radar (RIME instrument): when the spacecraft is protected from Jupiter radio emission

due to moon occultation for sources with frequency between 9 and 11 MHz (i.e., flybys and Ganymede phase) and when the spacecraft is within the RIME instrument operating range (altitude <1000km).

Data time	Event	Relative Time	in-situ	radio
2032-01-11T05:44:05	CA	-12:00:00	slow	full
2032-01-11T08:14:05	CA	-09:30:00	normal	full
2032-01-11T17:34:05	CA	-00:10:00	burst	full
2032-01-11T17:54:05	CA	+00:10:00	normal	full
2032-01-11T17:55:00	iono_ingress	+00:00:00	normal	burst
2032-01-11T18:01:00	iono_egress	+00:00:00	normal	full
2032-01-11T18:54:00	iono_ingress	+00:00:00	normal	burst
2032-01-11T19:11:00	iono_egress	+00:00:00	normal	full
2032-01-12T03:14:05	CA	+09:30:00	slow	full
2032-01-12T05:44:05	CA	-12:00:00	slow	full

Table 2. RPWI in-situ and radio observations mode sequence during the 21C13 Callisto flyby scenario. Some mode changes are scheduled w.r.t. Closest Approach event (CA), while ionosphere characterization observations are scheduled w.r.t ingress and egress events as identified using Express.

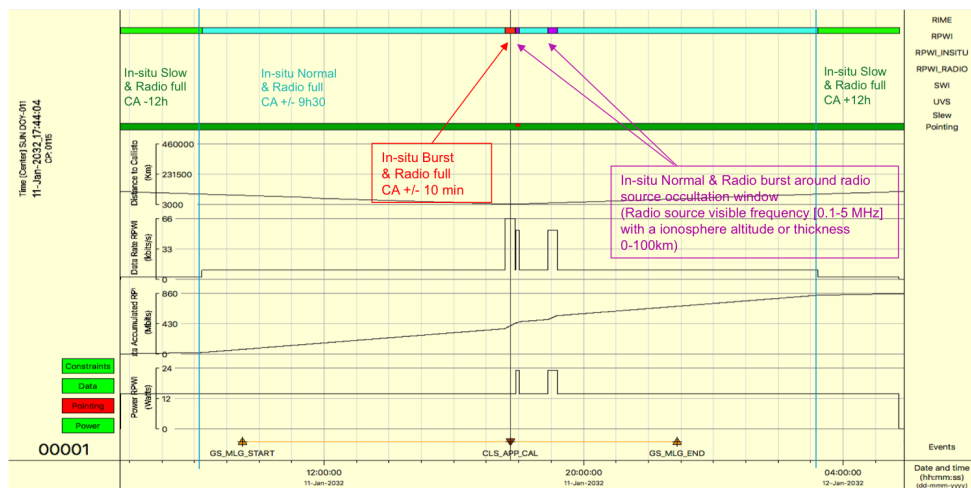


Fig. 14. This picture is a screenshot of this measurement sequences as shown by the JUICE SOC MAPPS tool, which allows to simulate the spacecraft and science instrument resources status (i.e., power, data rate, on-board memory). The top line is colour coded to reflect the different modes used by RPWI during the sequence. Instrument resources are displayed in the bottom plots.

7. Conclusions and Perspectives

The Galileo radio occultations observed on the PWS data set are well modeled by EXPRES simulation, with an accuracy of the order of one minute. Discrepancies between predicted and observed ingress or egress times can be attributed to refraction effects, which are not included in the current modeling scheme. The validation on GLL/PWS data allows us to apply the same modeling to the JUICE mission planning, in order to support the scientific segmentation of the Galilean moon flybys.

On a technical point of view, the JUICE modeling have been done running EXPRES through the PADC operated UWS interface based on OPUS. This framework is fully adapted to usage presented in this study. Future developments of the EXPRES code and its implementation at PADC will include better management of Provenance metadata (Servillat et al. 2020, 2021b), to enhance the scientific traceability and reproducibility of the results.

Several means of refining the occultation modeling have been identified. The main one is involving ray-tracing in the Jovian system (Io Torus) and the moon's environment. This extra modeling step requires models of the magnetic field and plasma density environments in the vicinity of the studied moon, including the magnetospheric and moon contributions. A second order improvement may also be provided by the use of a more accurate magnetospheric current sheet model, which will refine the location of the radio sources on the low frequency end.

Acknowledgments

The authors acknowledge support from Observatoire de Paris–PSL, CNRS, CNES and ESA for funding the research. The authors also acknowledge support from the Europlanet 2024 Research Infrastructure (EPN2024RI) project, which has received funding from the European Union's Horizon 2020 research and innovation programme under grant agreement No 871149). They want to emphasize the use of community developed tools and standards, which greatly facilitated this study (such as Autoplot, Das2, OPUS, UWS and Cosmographia and WebGeoCalc). They thank PADC for providing computing and storage resources. They also thank Marc Costa (from the NAIF SPICE team at NASA/JPL) for his very helpful feedback on configuring and using Cosomographia.

Appendix A: Equatorial Shadow Zone

In the equatorial region, in the innermost magnetosphere, the auroral radio sources are not visible, due to combination of the shape of the radio emission beaming patterns and the topology of the magnetic field lines bearing the radio source. This effect is named “Equatorial Shadow Zone” (ESZ). This effect has been identified at Saturn (Lamy et al. 2008), using a preliminary version of the ExPRES code. It has also been observed at Earth (see, e.g., Morioka et al. 2011, Figure 1), but not explicitly described.

Our simulation runs show that some of the Jovian auroral radio sources are not always visible at the distance of Io’s orbit. Figure A.1 shows the observability for each auroral radio source for an observer located on Io’s orbit, during one rotation of Jupiter. The simulation shows that the Southern radio sources (namely, the C and D source) are not visible in the CML range 180 to 210 degrees. The Northern radio sources (namely, the A and B source) are observable from all CML, with a drastically reduced spectral range at a CML of about 25 degrees. Since the Northern and Southern ESZs do not occur at the same time, an observer will not experience a full dropout of radio signals, contrarily to what is observed at Saturn.

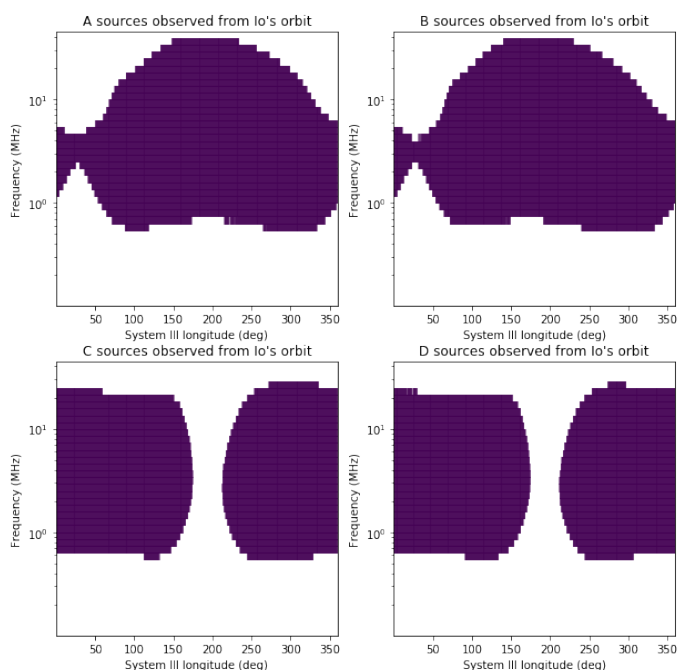


Fig. A.1. Jovian auroral radio source observability from Io’s orbit.

Appendix B: Supplementary Material Description

The material used to conduct the Galileo flybys’ study are provided as a separate data collection (Cecconi et al. 2021, available at <https://doi.org/10.25935/8zff-nx36>) hosted by PADC (Paris Astronomical Data Centre). For each flyby, two sets of material is available: (a) the ExPRES products; (b) the Cosmographia context products. The content of each subsection is described below.

Appendix B.1: ExPRES products

The ExPRES data set is composed of four files: (a) an ExPRES configuration file (JSON format), (b) a Galileo spacecraft

ephemeris data exported from WebGeoCalc (CSV format), (c) the output ExpRES simulation run data (CDF format), and (d) the observed GLL/PWS data with the superimposed occultation contours (PNG format). Files (a) and (b) contains the ExpRES parameters and the SPICE Kernels used for the simulation, ensuring the results are reproducible.

Appendix B.2: Cosmographia context products

The Cosmographia data set is composed of a series of subdirectories, organised according to Cosmographia’s documentation. It contains all the required configuration catalogue files: the SPICE catalogue file listing the kernels in use for a scene; the spacecraft catalogue file defining the time interval of the scene and the spacecraft reference frame; the modeled radio source catalogue file, derived from an ExPRES simulation run; the ExPRES configuration file and simulation run; and the scripts used to produce the movie output. Two output movies are provided, showing the flyby scenes, as seen from the spacecraft (‘pov’ labelled movie) and from the top of the Jovian system (‘top’ labelled movie).

References

- Acton, C., Bachman, N., Semenov, B., & Wright, E. 2018, *Planetary and Space Science*, 150, 9
- Acton, C. H. 1996, *Planet. Space Sci.*, 44, 65
- Bruzzone, L., Plaut, J. J., Alberti, G., et al. 2013, 2013 IEEE International Geoscience and Remote Sensing Symposium - IGARSS, 3907
- Burke, B. & Franklin, K. 1955, *J. Geophys. Res.*, 60, 213
- Cecconi, B. 2019, Workflow studies: Magnetospheres science and support to ESA/JUICE mission planning
- Cecconi, B., Hess, S., Hérique, A., et al. 2012, *Planet. Space Sci.*, 61, 32
- Cecconi, B., Loh, A., Le Sidaner, P., et al. 2020, *Data Science Journal*, 19, 1062
- Cecconi, B., Louis, C., Muñoz Crego, C., & Vallat, C. 2021, Auroral Radio Source Occultation Modeling and Application to the JUICE Science Mission Planning. Supplementary Material: Galileo Flybys
- Cecconi, B. & Zarka, P. 2019, Cassini RPWS Jupiter Encounter Calibrated Dataset
- Connerney, J. E. P., Acuna, M. H., & Ness, N. F. 1981, *Journal of Geophysical Research*, 86, 8370
- Connerney, J. E. P., Kotsiaros, S., Oliverson, R. J., et al. 2018, *Geophys. Res. Lett.*, 45, 2590
- ESA SPICE Service. 2020, JUICE SPICE Kernel Dataset
- Eviatar, A., Vasyliunas, V. M., & Gurnett, D. 2001, *Planet. Space Sci.*, 49, 327
- Gautier, A.-L., Cecconi, B., & Zarka, P. 2013, Proceedings of the 2013 International Symposium on Electromagnetic Theory, 1
- Grodent, D. 2015, *Space Sci. Rev.*, 187, 23
- Gurnett, D., Kurth, W. S., Menietti, J., & Persoon, A. 1998, *Geophys. Res. Lett.*, 25, 1841
- Gurnett, D., Kurth, W. S., Shaw, R., et al. 1992, *Space Sci. Rev.*, 60, 341
- Gurnett, D. A., Kurth, W. S., & Granroth, L. J. 1997, NASA Planetary Data System, GO-J-PWS-2-REDR-LPW-SA-FULL-V1.0 [<https://doi.org/10.17189/1519681>]
- Gurnett, D. A., Kurth, W. S., Roux, A., Bolton, S. J., & Kennel, C. F. 1996, *Nature*, 384, 535
- Harrison, P. A. & Rixon, G. 2016, Universal Worker Service Pattern Version 1.1, IVOA Recommendation 24 October 2016
- Hess, S. L. G., Echer, E., & Zarka, P. 2012, *Planetary and Space Science*, 70, 114
- Kliore, A. J. 1998, *Highlights of Astronomy*, 11B, 1065
- Kumamoto, A., Kasaba, Y., Tsuchiya, F., et al. 2017, in *Planetary Radio Emissions VIII*, ed. G. Fischer, G. Mann, M. Panchenko, & P. Zarka, 127–136
- Kurth, W. S., Bolton, S. J., Gurnett, D. A., & Levin, S. 1997, *Geophys. Res. Lett.*, 24, 1171
- Lamy, L., Zarka, P., Cecconi, B., Hess, S., & Prangé, R. 2008, *J. Geophys. Res.*, 113
- Lamy, L., Zarka, P., Cecconi, B., et al. 2017, in *Planetary Radio Emissions VIII*, ed. G. Fischer, G. Mann, M. Panchenko, & P. Zarka, 455–466
- Louarn, P., Allegrini, F., McComas, D. J., et al. 2017, *Geophys. Res. Lett.*, 44, 4439
- Louarn, P., Perraut, S., Roux, A., et al. 1997, *Geophys. Res. Lett.*, 24, 2115
- Louis, C. K., Hess, S. L. G., Cecconi, B., et al. 2019, *Astronomy and Astrophysics*, 627, A30

- Louis, C. K., Hess, S. L. G., Cecconi, B., et al. 2020, maserlib/ExPRES: Version 1.1.0, This work has also been supported by the EPN-2024-RI (Europlanet 2024 Research Infrastructure) project, under contract number 871149 with the EC.
- Marques, M. S., Zarka, P., Echer, E., et al. 2017, *Astronomy & Astrophysics*, 604, A17
- Menietti, J., Gurnett, D., Hospodarsky, G., et al. 2003, *Planet. Space Sci.*, 51, 533
- Morioka, A., Miyoshi, Y., Tsuchiya, F., et al. 2011, *Journal of Geophysical Research Space Physics*, 116, A04211 (15 pages)
- Piker, C., Granroth, L., Mukherjee, J., et al. 2019, *Earth and Space Science Open Archive* [<https://doi.org/10.1002/essoar.10500359.1>]
- Romero-Wolf, A., Vance, S., Maiwald, F., et al. 2015, *Icarus*, 248, 463
- Schroeder, D. M., Romero-Wolf, A., Carrer, L., et al. 2016, *Planetary and Space Science*, 134, 52
- Servillat, M., Aicardi, S., Cecconi, B., & Mancini, M. 2021a, arXiv e-prints, arXiv:2101.08683
- Servillat, M., Bonnarel, F., Louys, M., & Sanguillon, M. 2021b, arXiv e-prints, arXiv:2101.08691
- Servillat, M., Riebe, K., Boisson, C., et al. 2020, IVOA Provenance Data Model Version 1.0, IVOA Recommendation 11 April 2020
- Wahlund, J. E. 2013, in *European Planetary Science Congress, EPSC2013–637*
- Witasse, O. 2019, in *EPSC-DPS Joint Meeting 2019, Vol. 2019, EPSC–DPS2019–400*
- Zarka, P. 1992, *Adv. Space. Res.*, 12, 99
- Zarka, P., Cecconi, B., & Kurth, W. S. 2004, *J. Geophys. Res.*, 109, A09S15